AMERICAN ACADEMY OF OPHTHALMOLOGY®

A New Preclinical Model of Retinitis Pigmentosa Due to *Pde6g* Deficiency

Michelle Carmen Jentzsch, PhD,[1] *Stephen H. Tsang, MD, PhD,*[2,3] *Susanne Friederike Koch, PhD*[1]

Purpose: Retinitis pigmentosa (RP) is the most common cause of inherited blindness, with onset occurring as early as 4 years of age in certain rare but severe forms caused by mutations in the gamma subunit of phosphodiesterase 6 (PDE6). Studies in humans and mice have shown that RP pathology begins with progressive photoreceptor death, which then drives changes in downstream neurons, neighboring retinal pigment epithelium (RPE), and vasculature. Here, we present the first detailed analysis of RP disease progression in *Pde6g*-deficient mice.

Design: Experimental study of an RP mouse model.

Subjects: We studied *Pde6g*$^{-/-}$ and Pde6g$^{+/-}$ mice at the age of 7, 16, 30, 44, and 56 days with n = 2 to 5 per group and time point.

Methods: Photoreceptor degeneration and retinal remodeling were analyzed in retinal sections by immunofluorescence. Retinal blood vessel degradation was analyzed in flat-mounted retinas immunolabeled for isolectin GS-IB4. Protein expression was measured by immunoblot. Acellular capillaries were assessed in trypsin-digested and hematoxylin–eosin-stained retinas at postnatal day (P) 44. Retinal pigment epithelium cells were delineated in flat-mounted RPE-choroid-sclera by immunolabeling for the cell-adhesion protein β-catenin.

Main Outcome Measures: Immunofluorescence and morphometry (quantitative analysis of outer nuclear layer, dendrite area, vessel area, acellular vessels, RPE cell size, number of nuclei per RPE cell, RPE cell eccentricity, and RPE cell solidity).

Results: This novel RP model exhibits early onset and rapid rod degeneration, with the vast majority gone by P16. This pathology leads to retinal remodeling, including changes of inner retinal neurons, early activation of glia cells, degradation of retinal vasculature, and structural abnormalities of the RPE.

Conclusions: The pathology in our *Pde6g*$^{-/-}$ mouse model precisely mirrors human RP progression. The results demonstrate the significant role of the gamma subunit in maintaining phosphodiesterase activity and provide new insights into the disease progression due to *Pde6g* deficiency.

Financial Disclosure(s): Proprietary or commercial disclosure may be found after the references.

Supplemental material available at www.aaojournal.org.

Retinitis pigmentosa (RP) is the most common inherited retinal dystrophy worldwide, with 1 case for every 4000 people.[1] Retinitis pigmentosa is a progressive disease, with patients initially experiencing night blindness, followed by a gradual narrowing of the visual field (tunnel vision) and, ultimately, loss of daylight vision (color and fine acuity).[2] This clinical progression is mirrored by progressive cellular degeneration—first of the mutant rod photoreceptors that mediate night vision, followed by the secondary death of cone photoreceptors that mediate daylight vision.[3] This cell loss in the photoreceptor layer leads to remodeling in the neighboring inner retinal and retinal pigment epithelium (RPE) layers, as well as in blood vessels.[4] For example, remodeling of neurons in the inner nuclear layer includes retraction of bipolar cell dendrites, formation of new processes, and migration of surviving bipolar and amacrine cells into the photoreceptor or ganglion cell layers. In addition, Müller glia cells undergo reactive gliosis, forming a glial seal between the remnant neural retina and the RPE. Typically, gliosis is characterized by a dramatic increase in expression of glial fibrillary acidic protein and pronounced hypertrophy of Müller cells. Alterations of the RPE cells (e.g., RPE atrophy or pigmented bone spicules) and attenuation of the retinal blood vessels are also common secondary changes in human RP.[4,5]

Rod-specific phosphodiesterase 6 (PDE6), composed of alpha and beta catalytic subunits and 2 identical inhibitory gamma subunits,[6,7] is an essential component of the visual transduction cascade that, in response to light activation, regulates intracellular cyclic guanosine monophosphate levels by hydrolysis of cyclic guanosine monophosphate.[8] Mutations in any of the 3 PDE6 subunits can cause autosomal recessive RP in humans,[9] demonstrating that

https://doi.org/10.1016/j.xops.2023.100332
ISSN 2666-9145/23

each subunit is essential for photoreceptor function and maintenance.[9-11] Mutations in *PDE6A* and *PDE6B* are common, accounting for 5% to 8% of autosomal recessive RP cases.[12-14] On the other hand, mutations in *PDE6G* are rare[11] yet can lead to severe early-onset RP, with marked reduction in scotopic and photopic electroretinograms as early as 4 years of age.[11]

Loss of PDE6 function in mice also causes retinal degeneration that mimics the human phenotype, and numerous *Pde6a*- and *Pde6b*-deficient mouse models of RP have been used to study disease progression and remodeling as well as to develop therapies. In contrast, *Pde6g*-mutant mice ($Pdeg^{tm1/tm1}$, Del7C, Y84G, and W70A) have been mainly used to examine the effects of these mutations on photoreceptor degeneration and the activation and deactivation phases of phototransduction.[15] Significantly, the retinal pathology in *Pde6g*-mutant mice has not been analyzed. Here, we characterize a new PDE6G-deficient mouse model, $Pde6g^{CreERT2/CreERT2}$ (referred to as $Pde6g^{-/-}$), and use it to study the effect of *Pde6g* gene disruption on retinal morphology. We demonstrate very early and rapid degeneration of rod photoreceptor cells, with only a single row of cone photoreceptor nuclei remaining by postnatal day (P) 16. We also observed remodeling of inner retinal neurons, glial cell activation, decreased retinal vascularization, and abnormal RPE morphology. Thus, our $Pde6g^{-/-}$ mouse model faithfully replicates the progressive structural pathologies of human RP. More specifically, with its early onset and rapid time course, these mice model the devastating *PDE6G*-driven forms of human RP.

Material and Methods

Animals

Animal experiments were performed according to the Association for Research in Vision and Ophthalmology statement for the use of animals in ophthalmic and vision research and were approved by the local authorities. Mice were kept at a 12-hour light/12-hour dark cycle with access to water and food ad libitum. The $Pde6g^{CreERT2}$ mutation was generated in the Barbara & Donald Jonas Stem Cells Laboratory, Columbia University, by replacing exons 2 and 3 of the *Pde6g* gene with a CreERT2.[16] In our study, mutant mice ($Pde6g^{CreERT2/CreERT2}$, referred to as $Pde6g^{-/-}$) and control mice ($Pde6g^{CreERT2/+}$, referred to as $Pde6g^{+/-}$) of both sexes were used. Polymerase chain reaction primers used for genotyping were as follows:

Pde6g forward: 5′-GGTCAGATTCCAGTGTGTGGG-3′
Pde6g internal: 5′-CTTAGGTGGTCCTTTCCTGGG-3′
Pde6g reverse: 5′-GTTTAGCTGGCCCAAATGTTG-3′

Eye Preparation

Eyes were fixed in 4% paraformaldehyde in phosphate-buffered saline (PBS; pH, 7.4) for 5 min. The cornea and lens were removed, followed by a 40-min incubation in 4% paraformaldehyde. For cryosections, eyecups were washed 3 times in PBS (pH, 7.4), cryoprotected overnight in 30% sucrose at 4°C, and embedded in Tissue-Tek optimum cutting temperature compound (Sakura). Eyecups were frozen and sectioned vertically at 10 μm using a Leica CM3050S cryostat, collected on Thermo Scientific SuperFrost Plus slides, and stored at −20°C. For flat-mounted retinal and RPE-choroid-sclera preparations, eyecups were washed 3 times in PBS (pH, 7.4). The retina was separated, and RPE was bleached in 10% H_2O_2 for 1.5 hours at 55°C. For immunoblotting, retinas were removed and immediately frozen in liquid nitrogen.

Immunofluorescence

Retinal sections were stained in 5% ChemiBlocker (MerckMillipore #2170), 0.3% Triton-X-100 in PBS (pH, 7.4) overnight at 4°C using anti-Pde6g/h (Santa Cruz #sc-166350), anticone arrestin (Sigma # AB15282), anti-Pde6b (Invitrogen #PA1722), anti-secretagonin (gift from Prof. Dr Ludwig Wagner, University of Vienna, Austria), anticalbindin (Swant #300), antiprotein kinase c alpha (Santa Cruz #sc-8393), and antiglutamic-acid-rich protein (Sigma #MABN2429) primary antibodies. Flatmounts were stained in 5% ChemiBlocker, 3% dimethyl sulfoxide, and 0.3% Triton-X-100 in PBS (pH, 7.4) overnight at 4°C using anti-ionized calcium-binding adapter molecule 1 (Fujifilm Wako #019-19741) and anti-β-catenin (Cell Signaling #8480) primary antibodies or isolectin GS-B4 conjugated fluorescein (Sigma #L2895). Corresponding anti-Rabbit AF488 (Invitrogen #A-11070), anti-Rabbit AF647 (Invitrogen #A-21245), and anti-Mouse AF555 (Invitrogen #A-21425) secondary antibodies were incubated in 3% ChemiBlocker in PBS (pH, 7.4) for 1.5 hours at room temperature. Hoechst 33342 (Invitrogen #H1399) was used to stain nuclei. Samples were fixed with Aqua-Poly/Mount (Polysciences #18606) on Thermo Scientific SuperFrost Plus slides and stored at 4°C.

Trypsin Digestion and Hematoxylin–Eosin Staining

Retinal flatmounts were washed 5 times for 30 min in ddH_2O and incubated overnight at 4°C, followed by digestion in 3% trypsin (Thermo #27250018) in 0.1M Tris buffer (pH, 7.8) for 90 min at 37°C. The inner limiting membrane was removed with scissors in ddH_2O, and vasculature was cleaned by several washing steps. After drying, it was mounted on Thermo Scientific SuperFrost Plus slides and stained with the hematoxylin–eosin fast staining kit (Carl Roth #9194.1). Samples were fixed with Aqua-Poly/Mount.

Imaging and Quantification

Retinal sections were imaged with a Zeiss LSM710 confocal microscope. Images of retinal sections were taken in the ventral or dorsal area of the eye. Outer nuclear layer (ONL) thickness was measured 250 μm from the optic nerve using the Fiji software. Rod bipolar cell, horizontal cell, and cone bipolar cell dendrite areas close to the optic nerve were quantified as pixels in the outer plexiform layer using Fiji. Flatmounts were imaged as Z-Stack with a custom-made VisiScope CSU-X1 confocal system equipped with a high-resolution sCMOS camera (Visitron Systems) or with a Keyence BZ-X800 microscope using the sectioning tool. Relative vessel area was quantified using the AngioTool software.[17] Acellular capillaries were manually counted in brightfield images with equal size using Fiji. Retinal pigment epithelium cell morphology parameters were measured in images with equal size using CellProfiler 4.0.7. Nuclei per RPE cell were manually counted. All data were plotted using GraphPad Prism 9.3. Data are expressed as mean ± standard error of mean using an unpaired *t* test. $P \leq 0.05$ was considered statistically significant ($^*P \leq 0.05$; $^{**}P \leq 0.01$; $^{***}P \leq 0.001$). The N values refer to the number of individual animals.

Immunoblot

Retinae were lysed in M-PER Mammalian Protein Extraction Reagent (Thermo #78503) containing protease inhibitor (Sigma #11697498001) with a Branson Sonifier W-450D at 40% amplitude. Protein concentration was determined using the Pierce

Coomassie protein assay kit (Thermo #23200). Proteins (20 µg per sample) were separated by SDS-PAGE (Bio-Rad Mini Protean Tetra system) and transferred to a 0.2 µm polyvinylidene difluoride (PVDF) membrane (Sigma; GE10600021) for 2 hours at 120 V. Membranes were incubated in 5% nonfat dry milk in Tris-buffered saline with Tween20 for 1 hour at room temperature. Primary antibodies such as anti-Pde6g/h, antiglutamic-acid-rich protein, antiglial fibrillary acidic protein (Sigma #G3893), and anti-ß-actin-peroxidase (Sigma #A3854) were incubated in 5% nonfat dry milk overnight at 4°C. Corresponding anti-Mouse horseradish peroxidase (Santa Cruz # sc-516102) secondary antibody was incubated for 1 hour at room temperature. Proteins were detected using Immobilon Forte Western HRP substrate (Millipore #WBLUF0100) in a Bio-Rad ChemiDoc MP imager.

Results

Pde6g$^{-/-}$ Developing Mouse Retinas

In our *Pde6g*$^{-/-}$ mice, *Pde6g* exons 2 and 3 are replaced by *CreERT2* (Fig S1).[16] Heterozygous *Pde6g*$^{+/-}$ mice are used to drive tamoxifen-inducible, rod-specific Cre recombinase in order to carry out deletions at specific sites in the DNA.[16,18,19] To analyze the effect of PDE6G on postnatal development, we immunolabeled retinas from 7-day-old *Pde6g*$^{-/-}$ and *Pde6g*$^{+/-}$ (control) mice. It has already been shown that in P7 wild-type mice, photoreceptors are immature (i.e., rod and cone outer segments are very short) and programmed photoreceptor cell death is ongoing (i.e., the ONL is thicker than adult retina).[20] We first immunolabeled sections for PDE6G and found, as expected, immunolabeling in outer segments of *Pde6g*$^{+/-}$ retinas but not *Pde6g*$^{-/-}$ (Fig 2A). Since loss of a PDE6 subunit leads to reduced expression of the other 2 subunits,[21] we immunolabeled sections for PDE6B and found that, like PDE6G, PDE6B immunolabeling was not detectable in *Pde6g*$^{-/-}$ retinas (Fig 2A). To analyze rod outer segments and cones, sections were immunolabeled for N-terminal glutamic-acid-rich protein, which is a domain of rod cyclic nucleotide-gated beta1 channel subunit, and cone arrestin, respectively. Immunolabeling for both markers in *Pde6g*$^{-/-}$ and *Pde6g*$^{+/-}$ retinas was indistinguishable (Fig 2A). Rod and cone outer segments are still short as the first discs develop at approximately P7 in mice.[22,23] Finally, the mean ONL thickness was not significantly different in *Pde6g*$^{-/-}$ retinas (vs. *Pde6g*$^{+/-}$) ($P = 0.4$) (Fig 2B). These data suggest that, before P7, PDE6G has either no effect on gross morphological development or a very modest effect.

Progression of Photoreceptor Degeneration and Inner Retinal Remodeling in *Pde6g*$^{-/-}$ Retinas

We next analyzed the effects of PDE6G loss at later time points—P16, P30, and P44. As expected, PDE6G and PDE6B immunolabeling was not detectable in *Pde6g*$^{-/-}$ retinas at all time points but was intense in outer segments of *Pde6g*$^{+/-}$ retinas at P44 and P30 (Fig 3A, data not shown). At P16, PDE6G expression was less intense due to shorter rod outer segments of immature photoreceptors (data not shown).[22] In *Pde6g*$^{-/-}$ retinas, cones (arrestin immunolabeling) appeared as a single row of nuclei in the ONL at P16 as well as at P30 and were completely lost by P44 (Fig 3A). To quantify photoreceptor degeneration (rods and cones), ONL thickness was measured in retinal sections (Fig 3B). At P16 and P30, ONL thickness in *Pde6g*$^{-/-}$ retinas was already reduced by 87% and 92%, respectively, compared to age-matched *Pde6g*$^{+/-}$ retinas. By P44, all photoreceptor cells had died. In control *Pde6g*$^{+/-}$ retinas, the slight decrease in ONL thickness between P16 and P44 is due to normal programmed cell death of rods.[24]

Photoreceptor degeneration is accompanied by changes in downstream neurons.[25] To evaluate the time course of these changes in our *Pde6g*$^{-/-}$ mice, we visualized rod bipolar, horizontal, and cone bipolar neurons by immunostaining for protein kinase c alpha, calbindin, and secretagonin, respectively. In *Pde6g*$^{-/-}$ retinas, rod bipolar cell dendrites were shorter and less bushy along with thinning of the outer plexiform layer at P30, and at P44, most had disappeared. Horizontal cell processes underwent progressive retraction, which was evident at P30, and further progressed at P44. Cone bipolar cells and their dendrites (secretagonin) were shorter at P30; at P44, many cone bipolar cells had disappeared (Fig 3A). We next quantified the observed changes in rod bipolar cell dendrites, horizontal cell dendrites, and cone bipolar cell dendrites. At P16, there was no significant difference in the dendrite areas between *Pde6g*$^{+/-}$ and *Pde6g*$^{-/-}$ retinas. At P30, the dendritic areas were significantly reduced in *Pde6g*$^{-/-}$ compared with *Pde6g*$^{+/-}$ retinas. At P44, the dendritic areas were further decreased, reflecting the progressive retraction of dendrites (Fig 3C–E).

The absence of PDE6G and rod outer segments (glutamic-acid-rich protein) at P30 was further confirmed by immunoblotting (Figs 3F and S4). Because photoreceptor degeneration triggers reactive gliosis in Müller glial cells and chronic microglial activation, both were analyzed in our *Pde6g*$^{-/-}$ retinas. Reactive gliosis, analyzed by immunoblotting P30 retinal lysates, revealed dramatically increased glial fibrillary acidic protein expression in *Pde6g*$^{-/-}$ retinas (Fig 3F). Dramatic microglia/macrophage activation was revealed by increased ionized calcium-binding adapter molecule 1 immunolabeling in the center of P44 retinas (Fig 3G).

Thus, the loss of PDE6G leads to rapid degeneration of rod photoreceptor cells and secondary degeneration of cones (Fig 3A). The vast majority of rods degenerate between P7 (Fig 2B) and P16 (Fig 3A). At P30, rods are gone and few cones remain. At P44, all photoreceptors, including cones, have died (Fig 3A, B). Downstream neurons are already impacted by P16, with shorter and less complex processes (Fig 3A, C–E).

Retinal Blood Vessel Degeneration in *Pde6g*$^{-/-}$ Retinas

In mice, the retinal vasculature forms a trilaminar network of superficial, intermediate, and deep vascular plexuses. Following the loss of photoreceptors, this retinal vascular network decreases. In our *Pde6g*$^{-/-}$ mice (vs. *Pde6g*$^{+/-}$), we analyzed vascular changes in flat-mounted P16, P30, and P44 retinas immunolabeled for isolectin GS-IB4, an endothelial cell marker. The mean vessel area in deep and intermediate

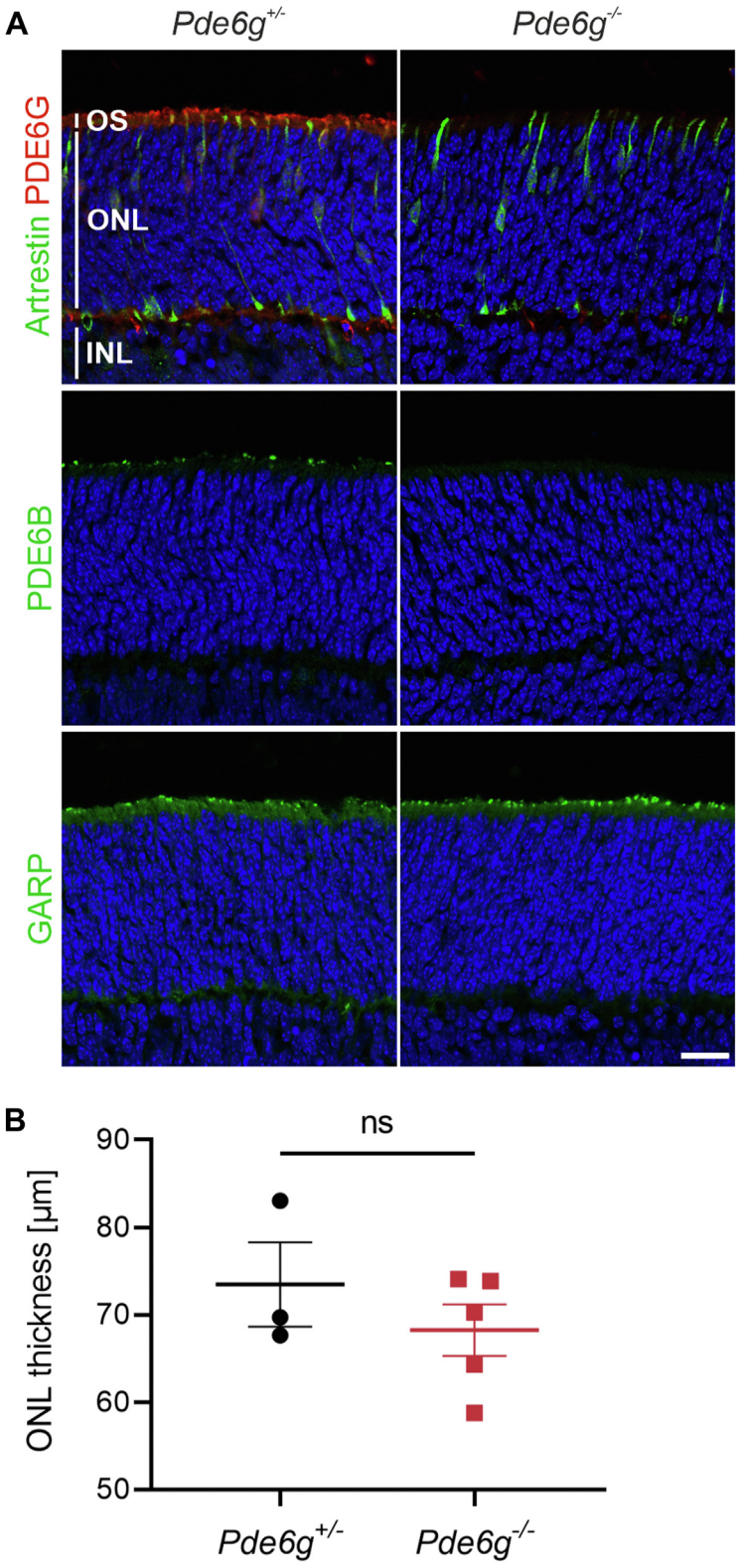

Figure 2. Morphological development of photoreceptors before postnatal day (P) 7 is not affected by phosphodiesterase 6 (PDE6G) depletion. Retinas were dissected from P7 *Pde6g*$^{+/-}$ (control) and *Pde6g*$^{-/-}$ (mutant) mice, sectioned, and immunolabeled. **A,** Representative images of sections stained for PDE6G and cone arrestin, PDE6B, or glutamic-acid-rich protein (GARP), and counterstained with Hoechst. **B,** Outer nuclear layer (ONL) thickness. Circles and squares, individual mice. *Pde6g*$^{+/-}$ (n = 3); *Pde6g*$^{-/-}$ (n = 5). Data are presented as the mean ± standard error of the mean and group means compared by an unpaired *t* test. Scale bar, 20 µm. INL = inner nuclear layer; ns = not significant; OS = outer segment.

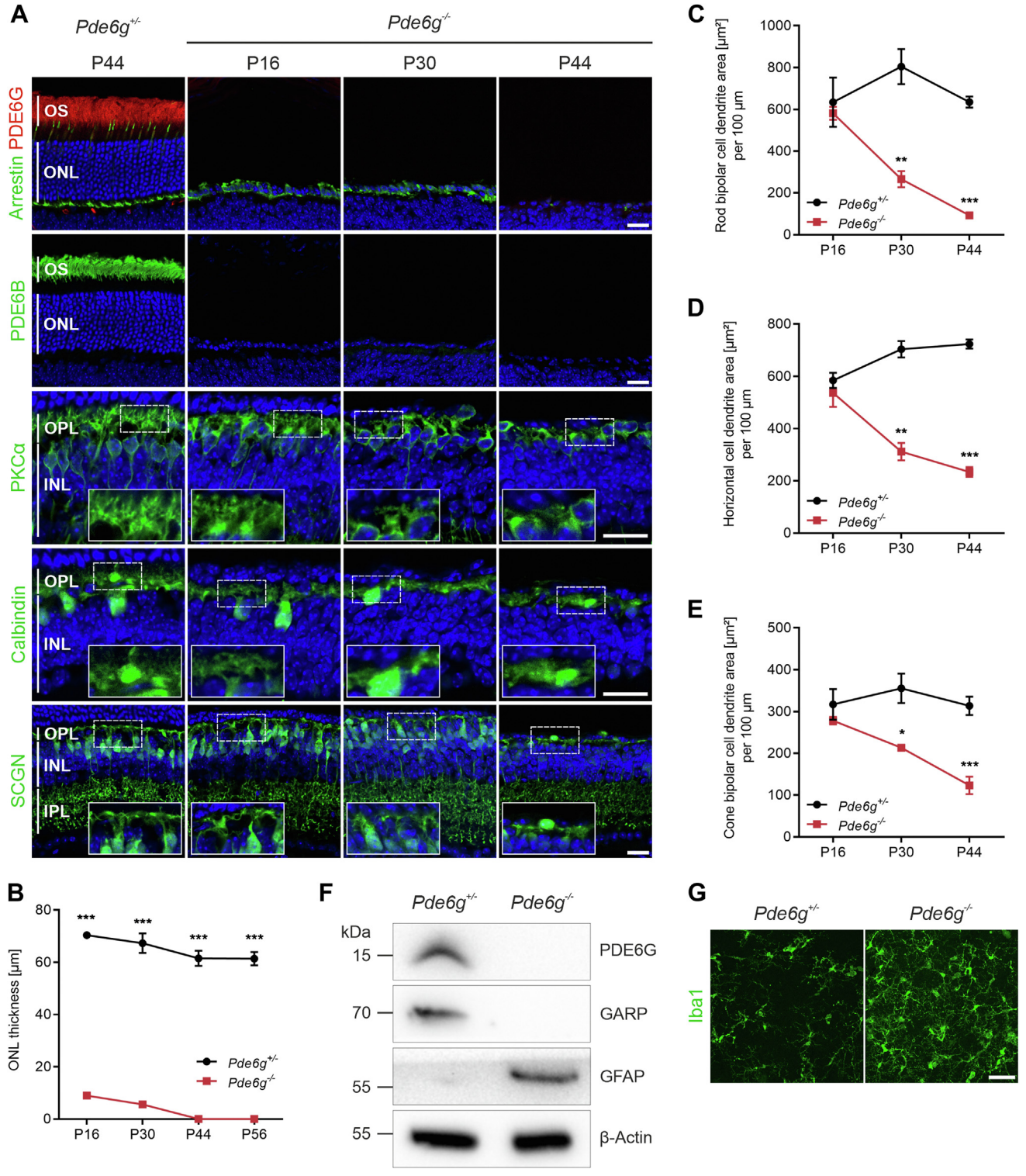

Figure 3. Loss of phosphodiesterase 6 (PDE6G) results in rapid photoreceptor degeneration and retinal remodeling. **A,** Representative images of retinal sections immunolabeled for PDE6G (rod outer segment [OS]), cone arrestin (cones), PDE6B (rod OS), protein kinase C alpha (PKCα) (rod bipolar cells), calbindin (horizontal cells), and secretagonin (SCGN) (cone bipolar cells) and counterstained with Hoechst. **B,** Outer nuclear layer (ONL) thickness of mice at postnatal day (P) 16 (n = 2–3), P30 (n = 3), P44 (n = 3), and P56 (n = 3–4). Circles and squares, individual mice. Data, presented as the mean ± standard error of the mean (SEM), were compared by unpaired *t* test. ***$P < 0.001$. **C–E,** Quantification of dendrite area from rod bipolar cells (**C**), horizontal cells (**D**), and cone bipolar cells (**E**) at P16 (n = 2–3), P30 (n = 3), and P44 (n = 4), respectively. Circles and squares, individual mice. Data, presented as the mean ± SEM, were compared by unpaired *t* test. *$P < 0.03$; **$P < 0.002$; ***$P < 0.001$. **F,** Representative immunoblot of P30 retinal lysates. β-actin, loading control. **G,** Representative images of microglia/macrophages in the center of P44 flat-mounted retinas immunostained for ionized calcium-binding adapter molecule 1 (Iba1). Scale bars, 10 µm. GARP = glutamic-acid-rich protein; GFAP = glial fibrillary acidic protein; INL = inner nuclear layer; IPL = inner plexiform layer; kDa = kilodalton; OPL = outer plexiform layer.

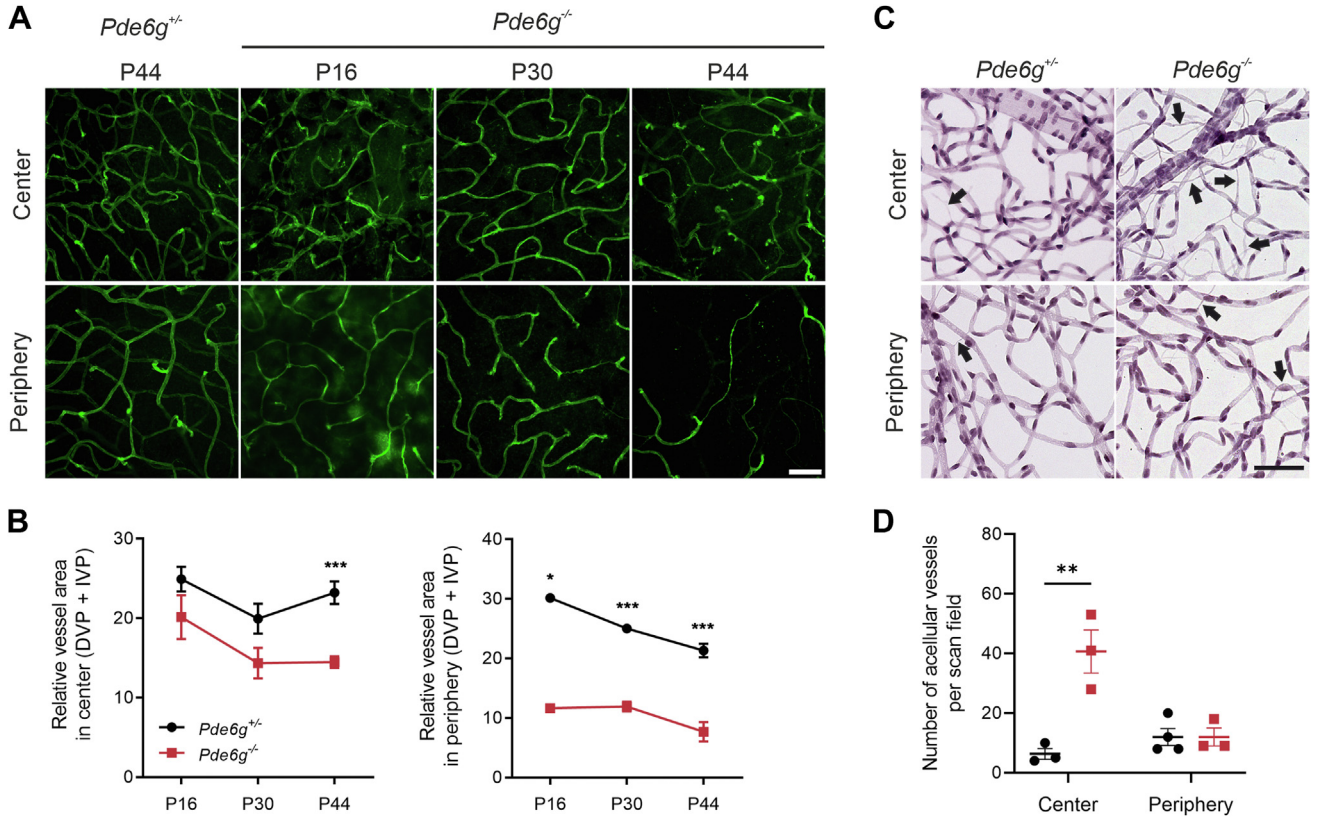

Figure 5. Retinal blood vessel degeneration in *Pde6g*$^{-/-}$ mice. **A,** Retinal flatmounts were immunostained for isolectin GS-IB4. **B,** Quantification of deep vascular plexus (DVP) + intermediate vascular plexus (IVP) blood vessel in retinal center and periphery: postnatal day (P) 16 (n = 2–3), P30 (n = 3–4), and P44 (n = 5). **C,** Retinas from P44 mice were flat-mounted, trypsin digested, and hematoxylin–eosin stained. Data presented as mean ± standard error of the mean. **D,** Quantification of acellular capillaries: *Pde6g*$^{+/-}$ (n = 3–4) and *Pde6g*$^{-/-}$ (n = 3). Circles and squares, individual mice. *Pde6g*$^{-/-}$ vs. *Pde6g*$^{+/-}$ age-matched group means were compared by unpaired *t* tests. **P* 0.02; ***P* 0.01; ****P* < 0.001. Scale bars, 50 μm.

vascular plexi was significantly reduced at all time points in peripheral retina. In central retinas, corresponding vessel area was again lower at all time points, but the difference was only significant at P44 (Fig 5A, B). In the superficial vascular plexus, vessel area was not changed at any time point in central or peripheral retinas (Fig S6).

When endothelial cells die, the result is acellular capillaries—nonperfused basement membrane sleeves with no endothelial cell nuclei along their length and an important marker for monitoring progression of RP. We assessed acellular capillaries at P44 in retinal flatmounts. While there were only small numbers of acellular capillaries in central and peripheral *Pde6g*$^{+/-}$ retinas, the numbers were significantly increased in central *Pde6g*$^{-/-}$ retinas (Fig 5C, D).

RPE Dysmorphia in *Pde6g*$^{-/-}$ Retinas

The RPE is a monolayer of columnar epithelial cells located between the retina and choroid, which is structurally and metabolically intertwined with the photoreceptor cell layer. Photoreceptor death in RP drives changes in the RPE.[26] To characterize these changes in our *Pde6g*$^{-/-}$ mice (vs. *Pde6g*$^{+/-}$), RPE cells were delineated in flat-mounted RPE-choroid-sclera by immunolabeling for the cell-adhesion protein β-catenin. As expected, RPE cells in *Pde6g*$^{+/-}$ mice were generally uniform in size and exhibited a polygonal (mostly hexagonal) shape (Fig 7A). Peripheral RPE from *Pde6g*$^{-/-}$ mice was generally indistinguishable from *Pde6g*$^{+/-}$ RPE, regardless of age (Fig 7A). In contrast, central RPE from *Pde6g*$^{-/-}$ mice was noticeably different from *Pde6g*$^{+/-}$ RPE—with minor morphological differences at P16 and P30 that were dramatic at P44. Essentially, the regular hexagonal geometry was replaced with polymorphous RPE of various, mostly elongated shapes. We next quantified these observations in RPE from P44 mice. The mean cell size was significantly smaller in *Pde6g*$^{-/-}$ (vs. *Pde6g*$^{+/-}$) RPE: 312 versus 388 μm^2 in the center and 261 versus 335 μm^2 in the periphery (Fig 7B). All RPE cells from *Pde6g*$^{-/-}$ and *Pde6g*$^{+/-}$ mice had either 1 or 2 nuclei, and there was no significant difference in the frequency of either cell type (Fig 7C). The number of nuclei per RPE cell was not significantly different between the 2 groups (Fig 7C). We also analyzed cell eccentricity (shape/elongation) and solidity (proportion of RPE cell area filling a best-fit convex envelope) (Fig 7D). Compared to control, *Pde6g*$^{-/-}$ RPE cells had significantly greater eccentricity centrally and significantly reduced solidity centrally and peripherally (Fig 7E, F).

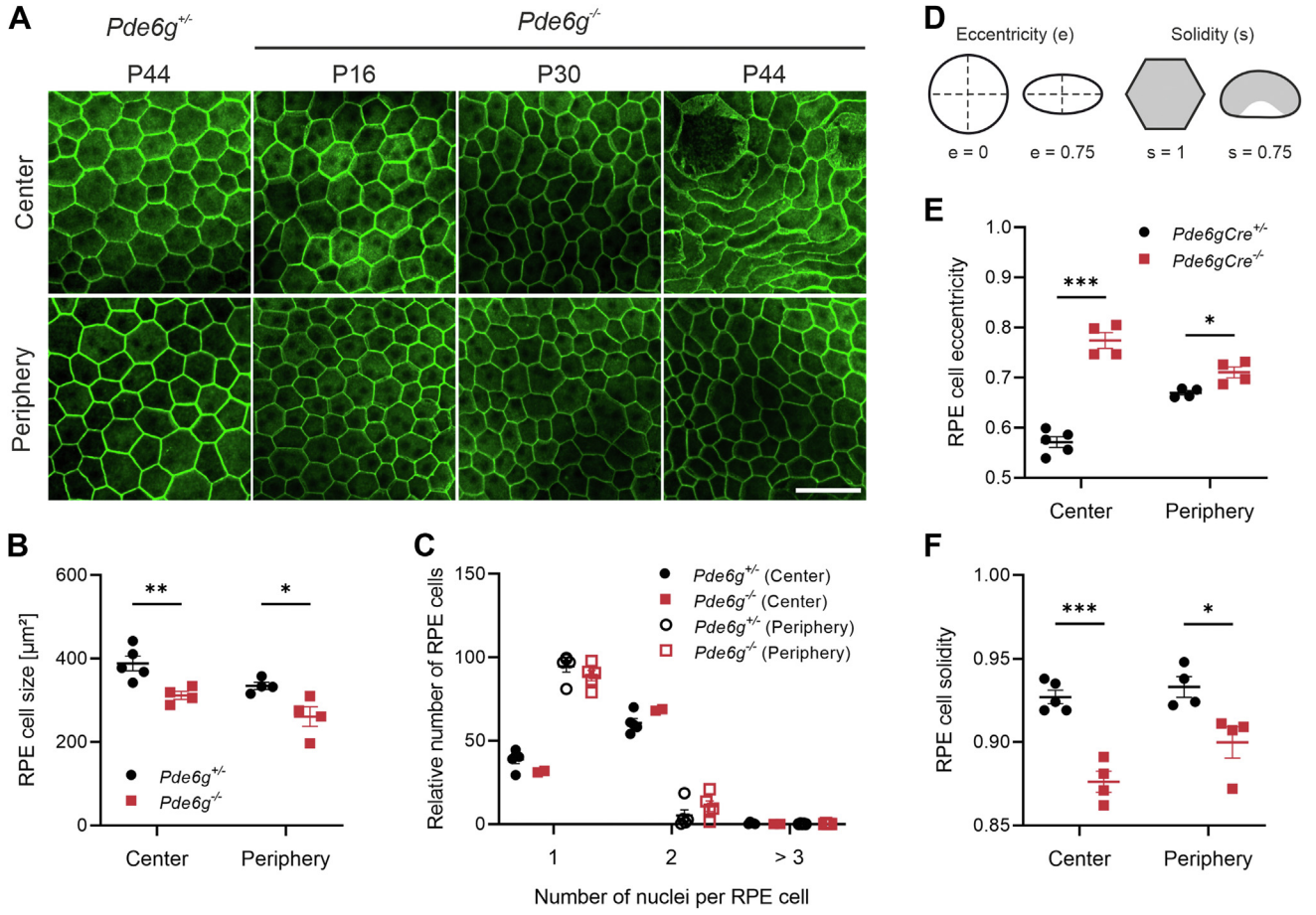

Figure 7. Retinal pigment epithelium (RPE) remodeling in *Pde6g*$^{-/-}$ mice. RPE-choroid-sclera preparations from *Pde6g*$^{+/-}$ mice at postnatal day (P) 44 and *Pde6g*$^{-/-}$ mice at P16, P30, and P44 were flat-mounted, immunostained for β-catenin, images were taken in center and periphery, and Z-Stacks merged. **A,** Representative immunofluorescence images. Scale bar, 50 µm. **B–F,** Quantification of RPE cell parameters from P44 mice. Circles and squares, individual mice. N values for *Pde6g*$^{+/-}$ and *Pde6g*$^{-/-}$ mice, respectively: (**B**, **D–F**) 4–5 and 4; (**C**) 5 and 2–4. Data presented as mean ± standard error of the mean. *Pde6g*$^{-/-}$ vs. *Pde6g*$^{+/-}$ age-matched group means were compared by unpaired *t* tests. **P* < 0.03; ***P* 0.01; ****P* < 0.001.

Discussion

Different variants in the same gene cause divergent RP disease progressions in humans and mice.[27,28] For example, mice carrying different alleles of *Pde6g* resulted in retinal phenotypes ranging from biochemical defects with no photoreceptor loss to severe photoreceptor degeneration.[15] In our *Pde6g*$^{-/-}$ mice, in which exons 2 and 3 of the *Pde6g* gene are replaced by *CreERT2*,[16] we observed a very early disease onset, extremely rapid loss of photoreceptors (the vast majority of rod photoreceptors are lost at P16), and no detectable PDE6B immunolabeling. Interestingly, the *Pde6g*$^{tm1/tm1}$ mouse line, in which the third exon was replaced with the bacterial neomycin resistance gene, shows a slightly later disease onset, a similarly rapid rate of photoreceptor degeneration (1 row of cone photoreceptors remaining at P21), and assembly, folding, and stability of the PDE6A/PDE6B complex does not appear to be affected.[29] In a third *Pde6g* mutant, deletion of the last 7 amino acids (Del7C) led to photoreceptor degeneration that was approximately 1 week slower than *Pdeg*$^{tm1/tm1}$ mice, and expression of PDE6A and PDE6B was reduced by approximately 90%.[30] Finally, mice carrying a point mutation in PDE6G at position 84 or 70 (Y84G or W70A, respectively) show no photoreceptor degeneration and normal expression of the 3 PDE6 subunits.[31,32] Thus, observations in these 5 *Pde6g* mutant mice suggest that the onset and rate of photoreceptor loss correlates with the strength of the genetically induced insult. This is consistent with the demonstration that residual PDE6A protein slows photoreceptor degeneration.[28]

In this study, we analyzed secondary changes in inner retinal neurons, glia cells, blood vessels, and RPE in response to photoreceptor loss in *Pde6g* mutant mice. In our *Pde6g*$^{-/-}$ mice, photoreceptor loss led to progressive morphological changes in second-order neurons, which were evident at P16 and included dendritic retraction and dislocation of the cell body of horizontal and rod and cone bipolar cells. Dendritic retraction, mostly of rod bipolar cells, has been previously described in *Pde6b* mutant mice (e.g., rd1 and rd10)[25,33,34] and in other retinal

degenerative mouse models.[35] Thus, it appears that photoreceptor loss, independent of the genetic cause, deafferents neural retina and induces negative plastic remodeling therein.[4]

Attenuation of retinal blood vessels is a characteristic clinical finding in both RP patients[5] and mouse models.[26,36,37] In our *Pde6g*$^{-/-}$ mice, we observed a significant decrease in vessel area in both center and periphery over time. The retinal vascular area in *Pde6g*$^{+/-}$ mice also becomes slightly reduced in the periphery which reflects remodeling processes that take place until adulthood (P120).[38] In *Pde6g*$^{-/-}$ mice, a significant decrease in vessel area at P16 in deep and intermediate vascular plexi in the peripheral retina but not in the superficial vascular plexus was detected. Thus, the early onset photoreceptor degeneration observed in our model impacts the development of the deep and intermediate plexi that form in the second and third postnatal weeks but not the superficial plexus that forms from P0 to P10.[39] In mutant rhodopsin Tg rat lines and rd1 mice that are characterized by partial loss of photoreceptor cells during development, partial failure of the deep vascular plexus development has been described.[36,40] A suggested mechanism for this reduced vascular development is increased oxygen tension driven by photoreceptor loss.[41,42] This idea is supported by research showing that developing retinal vasculature is reduced in hyperoxic conditions,[43] the inner retina becomes relatively hyperoxic following photoreceptor cell loss,[42] and the deep vascular plexus increases in an ambient hypoxic environment.[44]

We also analyzed secondary changes in RPE cells, which are structurally, functionally, and metabolically associated with photoreceptors.[45,46] Thus, when photoreceptors are compromised, RPE cells are impaired and undergo significant morphological changes.[26,47–49] This is the first study to examine correlations between RPE sheet morphology and photoreceptor degeneration in *Pde6g* mutant mice. In our *Pde6g*$^{-/-}$ mice, we observed minor changes in RPE at 16 or 30 days of age and dramatic abnormalities at 44 days, even though the vast majority of photoreceptors have degenerated at P16. In rd10 mutant mice, which carry a missense mutation (R560C) in *Pde6b*, rod degeneration begins around P18, peaks around P25, and at P45, RPE exhibits phenotypes that are not as severe as in our *Pde6g*$^{-/-}$ mice—compromised junctional complexes and both enlarged and abnormally small cells,[48] but at P100, there are major changes in RPE cell morphometrics.[50,51] Finally, in *Pde6g*$^{stop/stop}$ mice, which carry a STOP cassette in the *Pde6b* gene, photoreceptor degeneration has a late onset (beginning around week 4) and is slow, and dramatic changes in RPE morphology are first apparent around week 24.[26] These comparisons suggest that the age of onset for RPE remodeling is a function of the age of onset and speed of photoreceptor degeneration. These models also suggest that RPE remodeling appears sometime after photoreceptor loss, suggesting that bystander effects (e.g., oxidative stress, inflammation) require time to accumulate.[52] Last but not least, the small and elongated RPE cells in the center at P44 indicate that the RPE cells undergo dedifferentiation and epithelial−mesenchymal transition through β-catenin induction of mesenchymal genes.[53,54] The RPE dedifferentiation is a cardinal feature of the stress response[55] and has been implicated in several retinal diseases, including proliferative vitreoretinopathy, diabetic retinopathy, and age-related macular degeneration.[56] Thus, RPE cell survival in RP comes at the expense of epithelial attributes.

This preclinical mouse model and analysis describes the impact of a *Pde6g* mutation on RP disease progression and severity in multiple retinal layers. This study, in combination with analysis of other *Pde6a* and Pde6*b* mutants, as well as non-*Pde6* mutants, reveals the common and unique features of these mutants. This information can be used to develop therapeutic strategies for RP while also identifying potential therapeutic targets.

Acknowledgments

The authors thank Prof. Dr Ludwig Wagner for sharing the secretagonin antibody.

Footnotes and Disclosures

Originally received: November 11, 2022.
Final revision: May 5, 2023.
Accepted: May 8, 2023.
Available online: May 16, 2023. Manuscript no. XOPS-D-22-00244.

[1] Department of Pharmacy, Center for Drug Research, Ludwig-Maximilians-Universität München, Munich, Germany.

[2] Jonas Children's Vision Care, Columbia Stem Cell Initiative, Departments of Ophthalmology, Pathology and Cell Biology, Institute of Human Nutrition, Vagelos College of Physicians and Surgeons, Columbia University, New York, New York.

[3] Edward S. Harkness Eye Institute, New York-Presbyterian Hospital, New York, New York.

Disclosures:

All authors have completed and submitted the ICMJE disclosures form.

The authors made the following disclosures:

S.H.T.: Support − Abeona Therapeutics, Inc, Emendo; Scientific advisory panel − Nanoscope Therapeutics, Medical Excellence Capital; Founder − Rejuvitas. The remaining authors have no proprietary or commercial interest in any materials discussed in this article.

This work was supported by the German Research Foundation [Emmy Noether grant 5719/1−1] and the Daimler and Benz Foundation to S.F.K. Jonas Children's Vision Care is supported by the National Institute of Health 5P30CA013696, R01EY033770, R01EY018213, R01EY024698, R24EY027285, U01EY034590, U01EY030580, U54OD020351, R21AG050437, the Schneeweiss Stem Cell Fund, New York State [SDHDOH01-C32590GG-3450000] the Foundation Fighting Blindness TA-GT-0321-0802-COLU-TRAP, Nancy & Kobi Karp, the Crowley Family Funds, The Rosenbaum Family Foundation, Alcon Research Institute, the Gebroe Family Foundation, the Research to Prevent Blindness (RPB) Physician-Scientist Award, unrestricted funds from RPB, New York, NY.

HUMAN SUBJECTS: Animal experiments were performed according to the Association for Research in Vision and Ophthalmology statement for the use of animals in ophthalmic and vision research and were approved by the local authorities.

Author Contributions:

Conception and design: Jentzsch, Tsang, Koch

Data collection: Jentzsch

Analysis and interpretation: Jentzsch, Koch; Obtained funding: N/A

Overall responsibility: Jentzsch, Tsang, Koch

Abbreviations and Acronyms:
ONL = outer nuclear layer; **P** = postnatal day; **PBS** = phosphate-buffered saline; **PDE6** = phosphodiesterase 6; **RP** = retinitis pigmentosa; **RPE** = retinal pigment epithelium.

Keywords:
Retinitis pigmentosa, Remodeling, Retinal vasculature, Retinal pigment epithelium (RPE), PDE6G.

Correspondence:
Susanne Friederike Koch, PhD, Department of Pharmacy, Center for Drug Research, Ludwig-Maximilians-Universität München, Munich, Germany. E-mail: susanne.koch@cup.uni-muenchen.de.

References

1. Cross N, van Steen C, Zegaoui Y, et al. Current and future treatment of retinitis pigmentosa. *Clin Ophthalmol*. 2022;16:2909−2921.
2. Hartong DT, Berson EL, Dryja TP. Retinitis pigmentosa. *Lancet*. 2006;368(9549):1795−1809.
3. Hartong DT, Berson EL, Dryja TP. Retinitis pigmentosa. *Lancet*. 2006;368:1795−1809.
4. Jones BW, Pfeiffer RL, Ferrell WD, et al. Retinal remodeling in human retinitis pigmentosa. *Exp Eye Res*. 2016;150:149−165.
5. Milam AH, Li ZY, Fariss RN. Histopathology of the human retina in retinitis pigmentosa. *Prog Retin Eye Res*. 1998;17:175−205.
6. Baehr W, Devlin MJ, Applebury ML. Isolation and characterization of cGMP phosphodiesterase from bovine rod outer segments. *J Biol Chem*. 1979;254:11669−11677.
7. Hurley JB, Stryer L. Purification and characterization of the gamma regulatory subunit of the cyclic GMP phosphodiesterase from retinal rod outer segments. *J Biol Chem*. 1982;257:11094−11099.
8. Cote RH. Photoreceptor phosphodiesterase (PDE6): activation and inactivation mechanisms during visual transduction in rods and cones. *Pflugers Arch*. 2021;473:1377−1391.
9. McLaughlin ME, Ehrhart TL, Berson EL, Dryja TP. Mutation spectrum of the gene encoding the beta subunit of rod phosphodiesterase among patients with autosomal recessive retinitis pigmentosa. *Proc Natl Acad Sci U S A*. 1995;92:3249−3253.
10. Huang SH, Pittler SJ, Huang X, et al. Autosomal recessive retinitis pigmentosa caused by mutations in the alpha subunit of rod cGMP phosphodiesterase. *Nat Genet*. 1995;11:468−471.
11. Dvir L, Srour G, Abu-Ras R, et al. Autosomal-recessive early-onset retinitis pigmentosa caused by a mutation in PDE6G, the gene encoding the gamma subunit of rod cGMP phosphodiesterase. *Am J Hum Genet*. 2010;87:258−264.
12. Dryja TP, Rucinski DE, Chen SH, Berson EL. Frequency of mutations in the gene encoding the alpha subunit of rod cGMP-phosphodiesterase in autosomal recessive retinitis pigmentosa. *Invest Ophthalmol Vis Sci*. 1999;40:1859−1865.
13. Kim MS, Joo K, Seong MW, et al. Genetic mutation profiles in Korean patients with inherited retinal diseases. *J Korean Med Sci*. 2019;34:e161.
14. Oishi M, Oishi A, Gotoh N, et al. Comprehensive molecular diagnosis of a large cohort of Japanese retinitis pigmentosa and Usher syndrome patients by next-generation sequencing. *Invest Ophthalmol Vis Sci*. 2014;55:7369−7375.
15. Farber DB, Tsang SH. Stationary night blindness or progressive retinal degeneration in mice carrying different alleles of PDE gamma. *Front Biosci*. 2003;8:s666−s675.
16. Koch SF, Tsai YT, Duong JK, et al. Halting progressive neurodegeneration in advanced retinitis pigmentosa. *J Clin Invest*. 2015;125:3704−3713.
17. Lamprecht MR, Sabatini DM, Carpenter AE. CellProfiler: free, versatile software for automated biological image analysis. *Biotechniques*. 2007;42:71−75.
18. Koch SF, Duong JK, Hsu CW, et al. Genetic rescue models refute nonautonomous rod cell death in retinitis pigmentosa. *Proc Natl Acad Sci U S A*. 2017;114:5259−5264.
19. Zhang L, Cui X, Jauregui R, et al. Genetic rescue reverses microglial activation in preclinical models of retinitis pigmentosa. *Mol Ther*. 2018;26:1953−1964.
20. Sharma RK, O'Leary TE, Fields CM, Johnson DA. Development of the outer retina in the mouse. *Brain Res Dev Brain Res*. 2003;145:93−105.
21. Fu Y, Yau KW. Phototransduction in mouse rods and cones. *Pflugers Arch*. 2007;454:805−819.
22. Spencer WJ, Lewis TR, Phan S, et al. Photoreceptor disc membranes are formed through an Arp2/3-dependent lamellipodium-like mechanism. *Proc Natl Acad Sci U S A*. 2019;116:27043−27052.
23. Daum JM, Keles O, Holwerda SJ, et al. The formation of the light-sensing compartment of cone photoreceptors coincides with a transcriptional switch. *Elife*. 2017;6:e31437.
24. Young RW. Cell death during differentiation of the retina in the mouse. *J Comp Neurol*. 1984;229:362−373.
25. Strettoi E, Pignatelli V, Rossi C, et al. Remodeling of second-order neurons in the retina of rd/rd mutant mice. *Vis Res*. 2003;43:867−877.
26. Kajtna J, Tsang SH, Koch SF. Late-stage rescue of visually guided behavior in the context of a significantly remodeled retinitis pigmentosa mouse model. *Cell Mol Life Sci*. 2022;79:148.
27. Kim YN, Kim YJ, Seol CA, et al. Genetic profile and associated characteristics of 150 Korean patients with retinitis pigmentosa. *J Ophthalmol*. 2021;2021:5067271.
28. Sothilingam V, Garcia Garrido M, Jiao K, et al. Retinitis pigmentosa: impact of different Pde6a point mutations on the disease phenotype. *Hum Mol Genet*. 2015;24:5486−5499.
29. Tsang SH, Gouras P, Yamashita CK, et al. Retinal degeneration in mice lacking the gamma subunit of the rod cGMP phosphodiesterase. *Science*. 1996;272:1026−1029.
30. Tsang SH, Yamashita CK, Lee WH, et al. The positive role of the carboxyl terminus of the gamma subunit of retinal

cGMP-phosphodiesterase in maintaining phosphodiesterase activity in vivo. *Vis Res*. 2002;42:439–445.
31. Tsang SH, Yamashita CK, Doi K, et al. In vivo studies of the gamma subunit of retinal cGMP-phophodiesterase with a substitution of tyrosine-84. *Biochem J*. 2001;353:467–474.
32. Tsang SH, Burns ME, Calvert PD, et al. Role for the target enzyme in deactivation of photoreceptor G protein in vivo. *Science*. 1998;282:117–121.
33. Pang JJ, Dai X, Boye SE, et al. Long-term retinal function and structure rescue using capsid mutant AAV8 vector in the rd10 mouse, a model of recessive retinitis pigmentosa. *Mol Ther*. 2011;19:234–242.
34. Strettoi E, Pignatelli V. Modifications of retinal neurons in a mouse model of retinitis pigmentosa. *Proc Natl Acad Sci U S A*. 2000;97:11020–11025.
35. Baehr W, Frederick JM. Naturally occurring animal models with outer retina phenotypes. *Vis Res*. 2009;49:2636–2652.
36. Blanks JC, Johnson LV. Vascular atrophy in the retinal degenerative rd mouse. *J Comp Neurol*. 1986;254:543–553.
37. Hanna J, Yucel YH, Zhou X, et al. Progressive loss of retinal blood vessels in a live model of retinitis pigmentosa. *Can J Ophthalmol*. 2018;53:391–401.
38. Rust R, Gronnert L, Dogancay B, Schwab ME. A revised view on growth and remodeling in the retinal vasculature. *Sci Rep*. 2019;9:3263.
39. Dorrell MI, Aguilar E, Friedlander M. Retinal vascular development is mediated by endothelial filopodia, a preexisting astrocytic template and specific R-cadherin adhesion. *Invest Ophthalmol Vis Sci*. 2002;43:3500–3510.
40. Pennesi ME, Nishikawa S, Matthes MT, et al. The relationship of photoreceptor degeneration to retinal vascular development and loss in mutant rhodopsin transgenic and RCS rats. *Exp Eye Res*. 2008;87:561–570.
41. Matthes MT, Bok D. Blood vascular abnormalities in the degenerative mouse retina (C57BL/6J-rd le). *Invest Ophthalmol Vis Sci*. 1984;25:364–369.
42. de Gooyer TE, Stevenson KA, Humphries P, et al. Rod photoreceptor loss in Rho-/- mice reduces retinal hypoxia and hypoxia-regulated gene expression. *Invest Ophthalmol Vis Sci*. 2006;47:5553–5560.
43. Ashton N. Some aspects of the comparative pathology of oxygen toxicity in the retina. *Ophthalmologica*. 1970;160:54–71.
44. Penn JS, Li S, Naash MI. Ambient hypoxia reverses retinal vascular attenuation in a transgenic mouse model of autosomal dominant retinitis pigmentosa. *Invest Ophthalmol Vis Sci*. 2000;41:4007–4013.
45. Hurley JB. Retina metabolism and metabolism in the pigmented epithelium: a busy intersection. *Annu Rev Vis Sci*. 2021;7:665–692.
46. Strauss O. The retinal pigment epitheliumin visual function. *Physiol Rev*. 2005;85(3):845–881.
47. Boatright JH, Dalal N, Chrenek MA, et al. Methodologies for analysis of patterning in the mouse RPE sheet. *Mol Vis*. 2015;21:40–60.
48. Napoli D, Biagioni M, Billeri F, et al. Retinal pigment epithelium remodeling in mouse models of retinitis pigmentosa. *Int J Mol Sci*. 2021;22:5381.
49. Wu DM, Ji X, Ivanchenko MV, et al. Nrf2 overexpression rescues the RPE in mouse models of retinitis pigmentosa. *JCI Insight*. 2021;6:e145029.
50. Chrenek MA, Dalal N, Gardner C, et al. Analysis of the RPE sheet in the rd10 retinal degeneration model. *Adv Exp Med Biol*. 2012;723:641–647.
51. Jiang Y, Qi X, Chrenek MA, et al. Functional principal component analysis reveals discriminating categories of retinal pigment epithelial morphology in mice. *Invest Ophthalmol Vis Sci*. 2013;54:7274–7283.
52. Datta S, Cano M, Ebrahimi K, et al. The impact of oxidative stress and inflammation on RPE degeneration in non-neovascular AMD. *Prog Retin Eye Res*. 2017;60:201–218.
53. Zhou M, Geathers JS, Grillo SL, et al. Role of epithelial-mesenchymal transition in retinal pigment epithelium dysfunction. *Front Cell Dev Biol*. 2020;8:501.
54. Kim JW, Kang KH, Burrola P, et al. Retinal degeneration triggered by inactivation of PTEN in the retinal pigment epithelium. *Genes Dev*. 2008;22:3147–3157.
55. Zhao C, Yasumura D, Li X, et al. mTOR-mediated dedifferentiation of the retinal pigment epithelium initiates photoreceptor degeneration in mice. *J Clin Invest*. 2011;121:369–383.
56. Sripathi SR, Hu MW, Turaga RC, et al. Proteome landscape of epithelial-to-mesenchymal transition (EMT) of retinal pigment epithelium shares commonalities with malignancy-associated EMT. *Mol Cell Proteomics*. 2021;20:100131.